

How Jupiters save or destroy inner Neptunes around evolved stars

MARÍA PAULA RONCO,^{1,2} MATTHIAS R. SCHREIBER,^{3,2} CRISTIAN A. GIUPPONE,⁴ DIMITRI VERAS,^{5,6} JORGE CUADRA^{7,2}
AND OCTAVIO M. GUILERA^{8,1,2}

¹*Instituto de Astrofísica - Pontificia Universidad Católica de Chile, Av. Vicuña Mackenna 4860, Macul - Santiago, 8970117, Chile.*

²*Millennium Nucleus for Planet Formation, NPF, Chile.*

³*Instituto de Física y Astronomía, Universidad de Valparaíso, Valparaíso, Chile.*

⁴*Universidad Nacional de Córdoba, Observatorio Astronómico - IATE, Laprida 854, 5000 Córdoba, Argentina.*

⁵*Centre for Exoplanets and Habitability, University of Warwick, Coventry CV4 7AL, UK.*

⁶*Department of Physics, University of Warwick, Coventry CV4 7AL, UK.*

⁷*Departamento de Ciencias, Facultad de Artes Liberales, Universidad Adolfo Ibáñez, Avenida Padre Hurtado 750, Viña del Mar, Chile.*

⁸*Instituto de Astrofísica de La Plata, CONICET-UNLP, La Plata, Argentina.*

(Received May, 2020; Revised , 2020; Accepted February 1, 2022)

Submitted to ApJL

ABSTRACT

In about 6 Giga years our Sun will evolve into a red giant and finally end its life as a white dwarf. This stellar metamorphosis will occur to virtually all known host stars of exo-planetary systems and is therefore crucial for their final fate. It is clear that the innermost planets will be engulfed and evaporated during the giant phase and that planets located farther out will survive. However, the destiny of planets in-between, at $\sim 1 - 10$ au, has not yet been investigated with a multi-planet tidal treatment. We here combine for the first time multi-planet interactions, stellar evolution, and tidal effects in an N -body code to study the evolution of a Neptune-Jupiter planetary system. We report that the fate of the Neptune-mass planet, located closer to the star than the Jupiter-mass planet, can be very different from the fate of a single Neptune. The simultaneous effects of gravitational interactions, mass loss and tides can drive the planetary system towards mean motion resonances. Crossing these resonances affects particularly the eccentricity of the Neptune and thereby also its fate, which can be engulfment, collision with the Jupiter-mass planet, ejection from the system, or survival at a larger separation.

Keywords: planets and satellites: dynamical evolution and stability – stars: evolution – stars: mass-loss – methods: numerical

1. INTRODUCTION

More than 4000 exoplanets have been confirmed so far¹ and the discovered planetary systems, the vast majority around sun-like main sequence stars, reveal a great variety in terms of the number of planets, their masses, and orbital separations. These planetary systems are often referred to as the *final* outcome of planet forma-

tion, and are typically compared to the predictions of population synthesis analysis (Ronco et al. 2017; Morasini 2018) and/or N -body simulations (e.g. Pfyffer et al. 2015; Ronco & de Elía 2018).

However, the evolution of stars does not end on the main sequence and therefore neither does the evolution of the planetary systems around them. More than 100 gas giant planets² have been discovered around red giant stars (e.g. Jones et al. 2016) and convincing evi-

Corresponding author: M. P. Ronco, M. R. Schreiber
mronco@astro.puc.cl, matthias.schreiber@uv.cl

¹ (<http://exoplanet.eu/>, Schneider et al. 2011)

² <https://www.lsw.uni-heidelberg.de/users/sreffert/giantplanets/giantplanets.php>

dence for the existence of planetary debris and planets around white dwarfs has been provided in the last decades. About one third of all white dwarfs show atmospheric metal absorption lines that must result from the recent accretion of solid material (Koester et al. 2014). Roughly 5 per cent of these white dwarfs show a detectable infrared excess indicative of the presence of a circumstellar debris disk (Barber et al. 2012), and about the same fraction of the latter show a detectable gaseous disk component (Manser et al. 2020). As first suggested by Jura (2003), metal polluted white dwarfs and the disks around them are the result of the tidal disruption of rocky planetary material (Veras et al. 2014; Malamud & Perets 2020). In the spectacular case of the transiting and disintegrating planetesimal around WD 1145+017 we can witness this process in real time (Vanderburg et al. 2015; Gänsicke et al. 2016). Additional recent discoveries related to the final fate of planetary systems include a planetesimal which might resemble the core of an disrupted Earth-like planet orbiting a white dwarf in a close orbit (Manser et al. 2019) and a close-in Neptune-like planet that is evaporated by EUV irradiation from the white dwarf (Gänsicke et al. 2019) and was possibly tidally disrupted during its orbital decay (Veras & Fuller 2020). For hot white dwarfs, Schreiber et al. (2019) showed that the observed metal pollution (Barstow et al. 2014) can be explained if a large fraction (~ 50 per cent) of white dwarfs host planets at separations $\gtrsim 3$ au. This prediction is in line with the results of microlensing planet surveys that predict a large number of planets, mostly Neptunes, beyond the snow line (Suzuki et al. 2016).

Understanding the formation of planetary debris and the existence of planets around white dwarfs requires modelling the evolution of planetary systems beyond the main sequence (e.g. Veras & Gänsicke 2015). When the host star evolves into a giant star, each planet in a surrounding planetary system is subject to orbital changes. These changes are dominated by stellar tides and stellar mass-loss, particularly for planets inside ~ 10 au, although other mechanisms can have additional minor effects on the planetary orbits (see Veras 2016, and references therein). Stellar mass-loss tends to expand the orbit of the planets due to a decrease of the gravitational potential and simultaneous conservation of angular momentum but leaves the eccentricities nearly unchanged. Stellar tides, in contrast, tend to decrease both the semi-major axis and eccentricities of planetary orbits.

Several studies have determined the conditions under which *single* planets can survive the evolution of their host star into a white dwarf. However, the number of discovered planetary systems with more than just one

planet is continuously increasing (e.g. Shallue & Vanderburg 2018) and it seems plausible to assume that such systems might be the rule rather than the exception. It is then crucial to simulate the evolution of multiple planets affected by mass loss and stellar tides taking into account their mutual gravitational interactions. This has not been done yet.

We here close this gap by analysing the dynamical evolution of hypothetical planetary systems consisting of an inner Neptune- and an outer Jupiter-mass planet when their central star evolves through the Red Giant Branch (RGB) taking into account stellar mass-loss, stellar tides and the mutual gravitational interactions between the two planets. We find that under certain conditions the fate of the Neptune-mass planet is indeed significantly affected by the presence of the outer Jupiter-mass planet. Most interestingly, a Neptune-mass planet that would survive without a companion can be pushed into the giant star and a Neptune-mass planet that would not survive alone can be saved by the outer Jupiter.

2. PHYSICAL MODEL

In order to calculate the rate of change of the semi-major axis of a planet affected by the stellar mass-loss and stellar tides we adopt the formalism by Zahn (1977), which was also used by Villaver & Livio (2009) and Villaver et al. (2014). According to these authors, the change in orbital separation can be written as

$$\left(\frac{\dot{a}}{a}\right) = - \left(\frac{\dot{M}_\star}{M_\star + M_p}\right) - \left(\frac{\dot{a}}{a}\right)_t, \quad (1)$$

where M_\star is the total mass of the star, M_p the mass of the planet, a the semi-major axis of the planet's orbit, and $(\dot{a}/a)_t$ denotes the change of the semi-major axis caused by stellar tides given by:

$$\left(\frac{\dot{a}}{a}\right)_t = - \frac{1}{9\tau_{\text{conv}}} \frac{M_\star^{\text{env}}}{M_\star} \frac{M_p}{M_\star} \left(1 + \frac{M_p}{M_\star}\right) \left(\frac{R_\star}{a}\right)^8 \times \left[2p_2 + e^2 \left(\frac{7}{8}p_1 - 10p_2 + \frac{441}{8}p_3\right)\right]. \quad (2)$$

Here M_\star^{env} is the envelope mass and R_\star the radius of the star. We follow Rasio et al. (1996) to compute τ_{conv} , which is the eddy turnover timescale within the stellar envelope which writes as:

$$\tau_{\text{conv}} = \left[\frac{M_\star^{\text{env}} R_\star^{\text{env}} (R_\star - R_\star^{\text{env}})}{3L_\star}\right]^{1/3}, \quad (3)$$

where R_\star^{env} is the radius at the base of the convective envelope and L_\star the luminosity of the star. The frequency components of the tidal force, i.e. p_1 , p_2 and p_3

are, as in Mustill & Villaver (2012), given by:

$$p_i \approx \frac{9}{2} \min \left[1, \left(\frac{4\pi^2 a^3}{i^2 G (M_\star + M_p) \tau_{\text{conv}}^2} \right) \right], i = 1, 2, 3. \quad (4)$$

In a similar way, the eccentricity rate of change for the planet generated by tidal forces can be written as

$$\left(\frac{\dot{e}}{e} \right)_t = -\frac{1}{36\tau_{\text{conv}}} \frac{M_\star^{\text{env}}}{M_\star} \frac{M_p}{M_\star} \left(1 + \frac{M_p}{M_\star} \right) \left(\frac{R_\star}{a} \right)^8 \quad (5)$$

$$\times \left[\frac{5}{4} p_1 - 2p_2 + \frac{147}{4} p_3 \right].$$

Other mechanisms such as possible changes in the planet’s mass due to evaporation of its surface by EUV radiation or due to the accretion of a fraction of the ejected stellar material (Villaver & Livio 2009; Villaver et al. 2014), drag forces that occur when the planet passes through the gas expelled from the host star, and planetary tides, have been taken into account previously. However, these additional forces and the corresponding changes in the planet mass and orbital parameters are negligible compared to the effects of stellar mass-loss and stellar tides (Villaver & Livio 2009; Veras et al. 2015; Rao et al. 2018). We therefore only consider the latter.

3. NUMERICAL METHODS

In what follows we describe the numerical tools we used to calculate the evolution and fate of a Neptune-mass planet affected by the stellar mass-loss, stellar tides, and mutual gravitational interactions with a Jupiter-mass planet during the RGB.

3.1. The stellar evolution code

We use the stellar evolution code SSE developed by Hurley et al. (2000) which produces a single evolutionary track from a set of zero-age-main-sequence values such as the mass of the star M_\star , the metallicity Z , and the Reimers parameter η which controls the mass-loss rate (Reimers 1975). As we are only interested in the main effect of combining tidal forces, mass loss, and gravitational interactions we fixed the stellar evolution parameters to $M_\star = 1M_\odot$, $Z = 0.02$, and $\eta = 0.5$. The resulting evolutionary track provides information about the main parameters of the host star such as M_\star , R_\star , M_\star^{env} , R_\star^{env} and L_\star as a function of time from the zero-age-main-sequence and until the star becomes a white dwarf. Here we only discuss planetary system dynamics before and just beyond the tip of the RGB, during which the maximum radius achieved by the star is $\sim 186.34R_\odot$, equivalent to ~ 0.86 au, and the total stellar mass loss accumulates to $\sim 0.24M_\odot$. Analyses that include the AGB and WD phases will be presented in future papers.

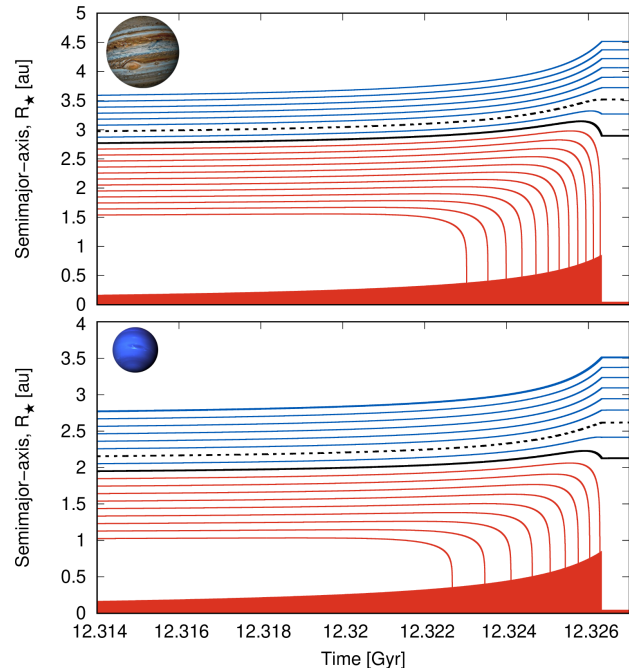


Figure 1. Evolution of the semi-major axis for a Jupiter (top) and a Neptune-mass planet (bottom) assuming initial separations of 1.5 – 3.5 au and 1 – 2.7 au, respectively with a step size of 0.1 au. Both planets are assumed to be in circular and coplanar orbits. The red filled area represents the radius of the host star for ~ 0.013 Gyr of its evolution towards the end of the RGB. The red solid lines show evolutionary tracks that result in an engulfment while the blue ones show those that lead to survival of the planets. The black solid line represents the limit between engulfment and survival (at 2.7 au for the Jupiter and at 1.9 au for the Neptune-mass planet) while the dashed line provides the limit above which tides are not strong enough to generate orbital decay at any time.

3.2. Evolution of a single planet

We calculated the evolution of a single planet using a Runge-Kutta Fehlberg (RKF) algorithm to integrate Eq. 1 coupled with Eq. 5 while taking into account the previously determined stellar evolution track. This numerical tool allows us to rapidly compute the fate of a single planet after the RGB for a range of initial orbital and planetary parameters. As an example, Fig. 1 shows the time evolution of the semi-major axis of a Jupiter (top) and of a Neptune-mass planet (bottom), located at different initial positions in circular and coplanar orbits.

We integrated the time evolution for initial separations between 1.5 au and 3.5 au for the Jupiter (top panel) and 1 au and 2.7 au for the Neptune-mass planet (bottom panel). The Jupiter-mass planets with an initial semi-major axis above 2.7 au survive while single

Neptune-mass planets survive for initial separations exceeding 1.9 au.

Although our model is simpler than previously performed simulations, our result for the survival of a Jupiter-mass planet with initial semi-major axis larger than 2.6 au is in agreement with more detailed numerical calculations. Using a different expression for the convective timescale, a different evolutionary track for the central star, and considering drag forces (which we ignored), Villaver & Livio (2009) found that a single Jupiter-mass planet around an evolving solar-mass star is engulfed for initial separations $a < 3$ au. According to Nordhaus & Spiegel (2013, their figure 3), who in addition to the most important forces considered changes in the primary spin, a Jupiter-mass planet around a solar-mass star would survive for initial separations exceeding $\sim 2.5 - 3$ au.

3.3. *N-body integrator*

To model the dynamics of a planetary system affected by stellar evolution we use the modified version of the MERCURY integration package (Chambers 1999) developed by Veras et al. (2013), which uses the Bulirsch Stoer (BS) integrator. This code interpolates the SSE code (Hurley et al. 2000) stellar mass output at each MERCURY time-step and at each BS substep, which produces the same single evolutionary track for a Solar-type star as the one used with the RKF integrator described in Sec. 3.2. For details about the computation of the mass-loss we refer the reader to Veras et al. (2013).

We implemented stellar tides in this version of MERCURY following the formalism described in Sec. 2 as an external force so that planetary evolution is affected not only by gravitational interactions between planets and with the central star, but also by dissipative effects. The description of the implementation of the stellar tides and its validation with the RKF integrations can be found in the Appendix.

4. RESULTS AND DISCUSSION

We analyze the evolution of a two-planet system formed by an inner Neptune and an outer Jupiter-mass planet. For simplicity, both planets are initially in circular and coplanar orbits. We calculated a grid with initial locations ranging from 2 to 3 au with a step size in separation of 0.1 au for the Jupiter and from 1.5 to 2.1 au with a step size of 0.05 au for the Neptune. This grid covers all combinations of fates obtained with the RKF integrations for single planets (engulfment–engulfment, engulfment–survival, survival–engulfment and survival–survival). For some of these semi-major axis pairs simulations are not performed because they violate the classical $\sim 3.5R_{\text{mH}}$ stability criteria (Gladman 1993), where

R_{mH} is the mutual Hill radius (see also Giuppone et al. 2013). For the rest of the angular orbital parameters we adopt random values between 0° and 360° . We integrate each configuration with both planets together for ~ 750 Myr starting at the base of the giant branch which according to SSE is reached by a star with one solar mass at an age of ~ 11.6 Gyr. We used an accuracy parameter of 1×10^{-13} (Veras et al. 2013) and saved the results every 1000 years. Collisions are treated as inelastic mergers, and close encounters are defined and recorded within 3 Hill radii.

Figure 2 illustrates the fate of both planets calculated with our *N*-body code as a function of initial separations. Especially for separations close to the 2:1 and 3:2 mean motion resonances (MMRs; white dashed lines) the fate of the inner Neptune-mass planet is dramatically affected by the presence of the outer Jupiter. We find four cases in which both planets fall to the central star despite the Neptune-mass planet would have survived the RGB on its own (see the red-red squares at $(a_J, a_N) = (2.5, 1.95)$, $(2.6, 1.85)$, $(2.6, 1.90)$ and $(2.6, 1.95)$ au). In two simulations the Neptune-mass planet collides with the Jupiter-mass planet (yellow squares in Fig. 2) before the latter is engulfed by the central star. These collisions occurred in cases where both planets alone would not have survived. We also find two cases where the Neptune-mass planet, which if it was on its own would have survived the RGB evolution of its host star, is ejected from the system due to close encounters with the outer Jupiter (small grey squares in Fig. 2). In one of these cases the Jupiter-mass planet survives while in the other one it is engulfed by the giant star.

The perhaps two most intriguing scenarios are, however, the following. On one hand, we find “saviour cases” in which the Neptune-mass planet alone would not survive the RGB but is saved by its Jupiter-mass companion (two cases, small blue square above big red square for red numbers on the y-axis in Fig. 2). On the other hand, we also find “destroyer cases” where the Neptune-mass planet alone would not have been engulfed by the giant star but is killed by the outer Jupiter (six cases, small red square above big blue square for blue numbers on the y-axis in Fig. 2). It is important to highlight that all these particular cases occur near the 3:2 and 2:1 MMR which cross the grid of the chosen semi-major axis. This does not imply that these cases are unlikely outliers. In contrast, Nature seems to have a preference for locating two consecutive planets close to the 3:2 and 2:1 MMR (e.g. Fabrycky et al. 2012; Trifonov et al. 2014). That such a configuration can be destabilized during the RGB causing one of the planets to be ejected has previously been predicted by Voyatzis et al. (2013)

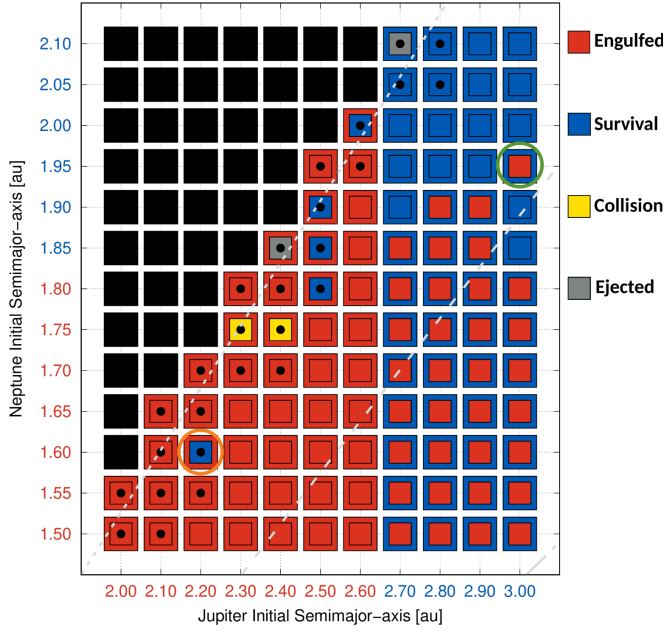


Figure 2. Final fate of the Jupiter (large squares) and the Neptune-mass planet (small inner squares) as a function of their initial separations. Red squares indicate the planet is engulfed by the central star, grey denotes the planet is ejected, blue means the planet survives, and yellow means the planet collides with the larger one. The black dots in the centre of some of the squares highlight those simulations in which close encounters (defined within 3 Hill radii) took place, and the grey long and short dashed lines show the positions of the 2:1 and the 3:2 MMR, respectively. The numbers providing the initial semi-major axis of both planets are coloured in red or blue, depending on whether they would survive or be engulfed as single planets. The filled black squares represent combinations that are unstable. Two of the cases where the presence of the outer planet changes the fate of the Neptune-mass planet are highlighted with green and orange circles.

who, however, did not take into account stellar tides. Finally, we emphasize that due to the stochasticity of the passage through the separatrix of the resonances, the results presented here can have different endings if the initial conditions are slightly changed, if a different timestep is considered, or even if a different computer is used (Voyatzis et al. 2013; Folonier et al. 2014).

4.1. Destroyer and Savior scenarios

The “destroyer” and “saviour” cases are fascinating scenarios that deserve a more detailed look. To that end we show the evolution of the separation and eccentricity for both cases as well as dynamical maps in Fig. 3. To construct the dynamical maps we set the Jupiters at their initial semi-major axis (3 and 2.2 au) and their eccentricity at its mean value attained in the first 100 Myr of the N-body integrations ($\sim 5 \times 10^{-4}$). The (a_N, e_N)

plane was then divided in a 100×100 grid of initial conditions for the Neptune-mass planet. The semi-major axis ranged from 1.7 to 2 au (left panel, “destroyer” case) and 1.55 to 1.75 au (right, “saviour”) and the eccentricity from 0 to 0.2. All these configurations were then integrated for 10,000 yr with the Neptunes represented by mass-less particles and without considering stellar tides and stellar evolution.

In the “destroyer” case (panels a, c and e of Fig. 3) the surviving Jupiter causes the death of the Neptune-mass planet that would have survived the evolution of their host star on the RGB if it was alone (the simulation with a green circle in Fig. 2). Throughout the integration the planets do not experience close encounters. The evolution corresponds to a divergent migration as the period ratio increases. At first, the Neptune’s eccentricity only slightly grows as their period ratio increases but instantly jumps to ~ 0.15 as soon the planets cross the 2:1 resonance (see panels a and c of Fig. 3). This increase in eccentricity causes the perihelion distance of the Neptune to significantly shrink. Stellar tides become more important at these smaller distances which further reduces the separation until the planet finally falls into the envelope of the giant star.

In the “saviour” case the opposite occurs, i.e. the Neptune-mass planet survives although it would not if it was alone (simulation with an orange circle in Fig. 2). In this scenario, shown in detail in panels b, d and f of Fig. 3, the Jupiter-mass planet is initially set on a highway to hell and will indeed fall into the giant star, but not without saving its Neptune-mass companion.

Despite their period ratio being initially far from the nominal value of the 3:2 MMR (i.e. $P_J/P_N \sim 1.5$), the initial planet locations are within this resonance. As a consequence, both planets evolve due to stellar tides following the apsidal corotation families, the bluish region in panel e where $\Delta_e \sim 0$, (see also Giuppone et al. 2013; Ramos et al. 2015). The migration in this case is convergent as the period ratio decreases. When the planets cross the 8:5 MMR, the Neptune’s eccentricity is slightly enhanced but then remains constant for the next $\sim 50,000$ yr. Then, both planets continue evolving towards shorter separations (and period ratios) as stellar tides dominate over the effects of stellar mass loss until they get trapped in the 3:2 MMR. This trapping increases the Neptune’s eccentricity to ~ 0.15 which leads to close encounters between both planets. Just ~ 0.8 Myrs before the star reaches the tip of the RGB a planetary scattering event occurs during which the Neptune is kicked to an orbit with $a \sim 3.20$ au and $e \sim 0.40$. As the star is still losing mass and as at the increased orbital distance stellar tides are very inefficient, the Nep-

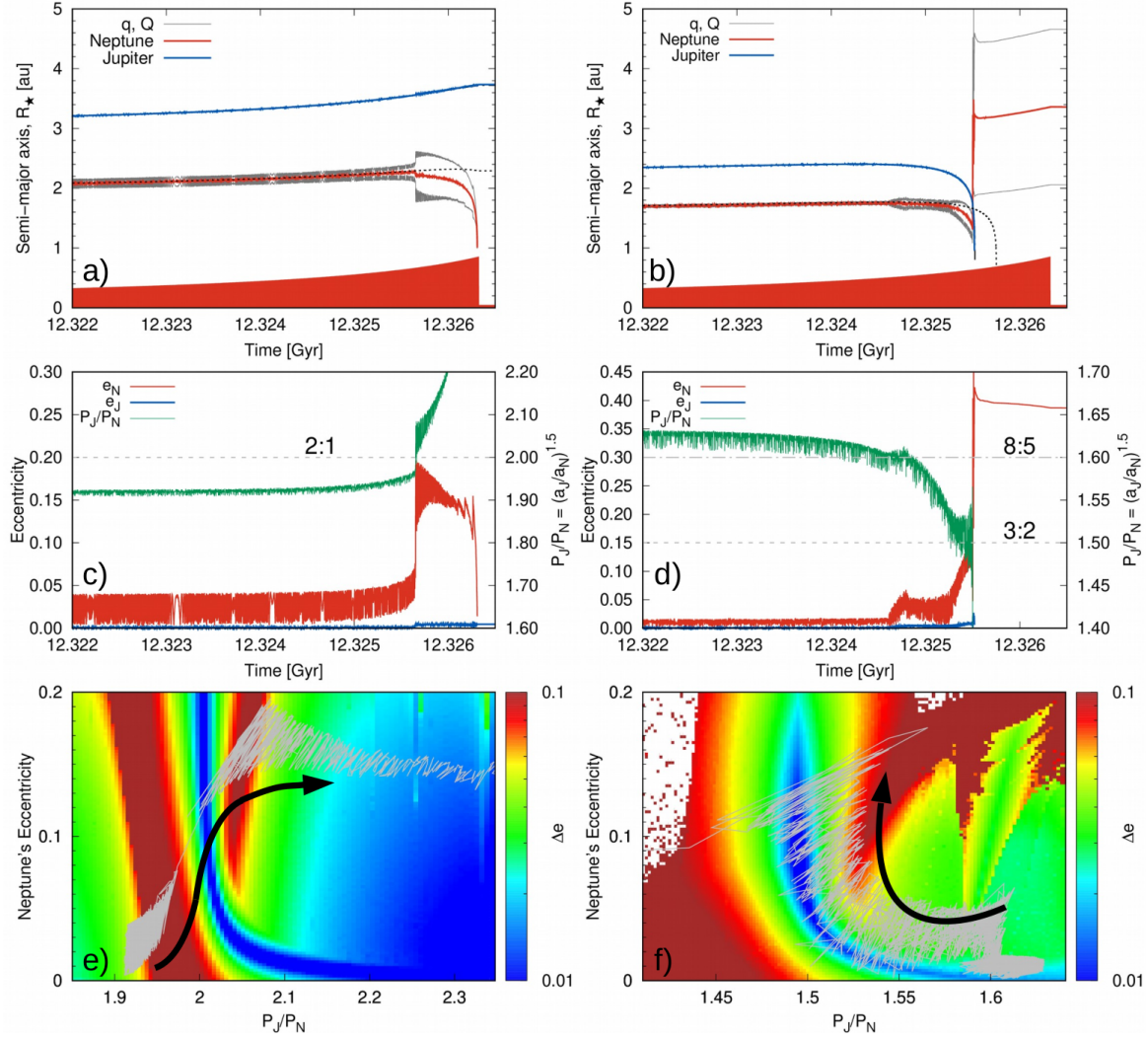


Figure 3. A detailed look at the “destroyer” (left) and the “saviour” (right) cases. The panels a and b show the time evolution of the Jupiter (blue) and the Neptune (red) semi-major axis for initial values of 3 and 1.95 au (left) and 2.2 and 1.6 au (right). The grey curves represent the Neptune’s perihelion and aphelion, the short and long dashed lines the evolution if the planets were single. Panels c and d show the evolution of the eccentricities of both planets and their period ratio, with the location of the 2:1 MMR (left) and the 3:2 and 8:5 MMR (right) indicated by dotted lines. The bottom panels e and f show the corresponding dynamical maps. The colorscale represents the Δe values in the $(P_J/P_N, e)$ plane for initial conditions in the vicinity of the 2:1 (left) and 3:2 MMR (right). Our N-body integrations are displayed by the grey lines. On the right (“saviour”) the evolution is convergent (period ratio decreases) and e increases as the system follows the 3:2 MMR. This leads to close encounters and finally the scattering event that saves the Neptune. In contrast, the evolution is divergent on the left and e increases as the system crosses the 2:1 MMR. This causes the perihelion distance to decrease, tidal forces to increase, and finally the planet to fall into the star.

tune’s orbit expands further until the tip of the RGB reaching final orbital parameters of $a \sim 3.31$ au and $e \sim 0.37$.

4.2. Neptune RGB survivors

Inspecting the final orbital parameters of the surviving Neptune-mass planets from all the simulations shown in Fig. 2, we identify two different populations as illustrated in Fig. 4. Surviving Neptunes with semi-

major axis greater than 3 au and eccentricities larger than ~ 0.25 result from planetary scattering events like the one described in the right panels of Fig. 3, while those with lower eccentricities and semi-major axes result from gravitational interactions and resonance crossings that enhanced their eccentricities but not enough to push them towards the star, as in the case of Fig. 3 (left panels).

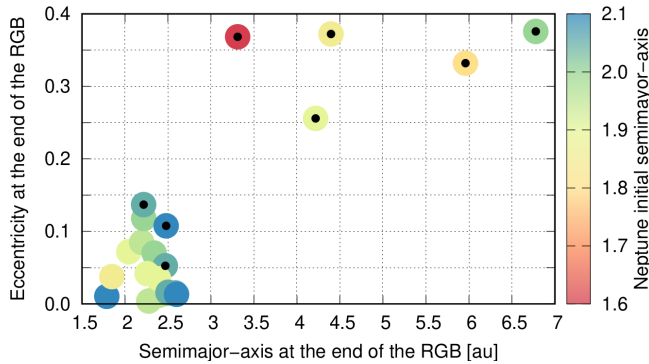


Figure 4. Semi-major axis vs eccentricity plane for the surviving Neptunes of Fig. 2. The Neptunes with black dots suffered close encounters with the Jupiter-mass planet.

Our findings therefore show that a significant fraction of planetary systems around white dwarfs might be shaped by gravitational interactions, in particular resonances, occurring during the evolution of their host stars. Eccentric orbits of planets around white dwarfs generated this way might play a significant role in scattering planetesimals or asteroids (Frewen & Hansen 2014; Smallwood et al. 2018; Antoniadou & Veras 2019) and maybe even smaller planets closer to the white dwarf. It could therefore be that the evolutionary scenarios discovered in this letter represent an important ingredient for understanding metal polluted white dwarfs as well as the properties of planetary systems around white dwarfs.

However, so far we have only considered two-planet systems while packed planetary systems with more planets might be a frequent outcome of planet formation (Gillon et al. 2017). In fact, the most recent measurements indicate that on average planetary systems consist of more than three planets (Zhu et al. 2018; Zink et al. 2019). In addition, our simulations only covered the first giant branch while the progenitors of all currently known white dwarfs must have evolved as well through the AGB which would likely affect some of the systems considered here (Mustill & Villaver 2012). Finally, we only considered planets around a $1M_{\odot}$ star while most of the observed metal-polluted white dwarfs have more massive progenitors (Koester et al. 2014) which suffer most of the radius expansion and mass-loss during AGB. We plan to overcome these limitations in future papers.

5. CONCLUSIONS

For the first time we combined stellar tides and multi-planet dynamics in an N -body code to study the evolution of a Neptune–Jupiter planetary system during the giant branch phases. We find that the fate of the Neptune-mass planet, located inside the Jupiter’s orbit, can be significantly affected by the presence of the Jupiter-mass planet during and after the evolution of the host star on the RGB. When both planets are near a MMR, the eccentricity of the Neptune-mass planet is excited which affects its fate: Planets that would survive alone can be engulfed by the giant star and planets that would fall into the giant star if they were on their own can survive due to planet–planet scattering events. We also observe an increased eccentricity of Neptune-mass planets that survive the RGB evolution of their host star. While additional simulations covering different stellar and planetary masses and including AGB evolution are required, our results clearly show that gravitational interactions play an important role for fate of planets that are initially located at a few au from the star. In particular, resonances between planetary orbits occurring during the stars giant phases might be crucial to understand the architecture of planetary systems around white dwarfs.

ACKNOWLEDGMENTS

We thank the anonymous referee for suggesting improvements to the manuscript. MPR thanks Marcelo M. Miller Bertolami for useful discussions on stellar evolution aspects. MPR and MRS acknowledge support from FONDECYT (grants 3190336 and 1181404). MPR, MRS, JC and OMG are supported by the Iniciativa Científica Milenio (ICM) via the Núcleo Milenio de Formación Planetaria. MPR also thanks CONICYT project Basal AFB-170002. OMG is partially supported by PICT 2016-0053 from ANPCyT, Argentina, and thanks IA-PUC for an invited research stay. DV gratefully acknowledges the support of the STFC via an Ernest Rutherford Fellowship (grant ST/P003850/1). CG acknowledges Mulatona Cluster from CCAD-UNC, which is part of SNCAD-MinCyT, Argentina.

APPENDIX

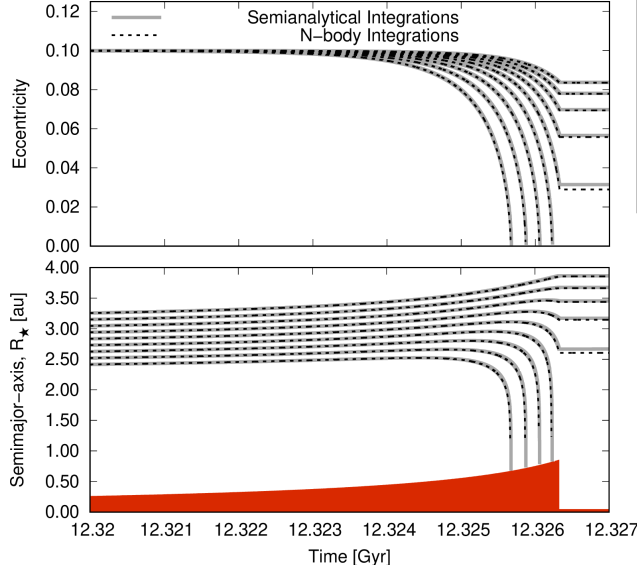


Figure 5. Comparison between evolution of the semi-major axis (bottom) and the eccentricity (top) of different orbits of a Jupiter-mass planet developed with the RKF integrator (grey solid line) and with the MERCURY N -body code (black dashed line). The red filled area represents the radius of the host star only for the last 6 Myr of its evolution towards the end of the RGB.

A. IMPLEMENTATION OF STELLAR TIDES

Different types of external forces affecting the evolution of a planet, like tides, interactions with a planetesimal disk, or disk torques, can be modeled by a Stokes non-conservative force as:

$$\frac{d^2 \mathbf{r}}{dt^2} = -C(\mathbf{v} - \alpha \mathbf{v}_c) \quad (\text{A1})$$

(Beaugé et al. 2006). Here \mathbf{r} is the position vector referring to the star, \mathbf{v} is its velocity vector and \mathbf{v}_c is the circular velocity vector at the same point. C and α are external coefficients. At first order in eccentricity and for a single planet, the effects of the previous force in the semi-major axis and eccentricity of the body can be described following Beauge & Ferraz-Mello (1993):

$$a(t) = a_0 \exp(-At), \quad e(t) = e_0 \exp(-Et) \quad (\text{A2})$$

where a_0 and e_0 are the conditions at the beginning of the integration and where $|A|$ and $|E|$ represent the inverse of the e-folding times for a and e , which can be computed as:

$$A = 2C(1 - \alpha), \quad E = C\alpha. \quad (\text{A3})$$

To the first order, we can assume the right-hand sides of equations 2 and 5 as constant. Then, their solutions are formally given by Eq. A2, and $A = \left(\frac{\dot{a}}{a}\right)_t$ and $E = \left(\frac{\dot{e}}{e}\right)_t$ can be used to deduce the coefficients C and α as:

$$C = \frac{1}{2}A + E, \quad \alpha = \frac{E}{C}. \quad (\text{A4})$$

Following this formalism the accelerations from tides were incorporated in our N -body code.

In order to test this implementation in MERCURY we evolved a single planet system until the central Solar-mass star passed through the tip of the RGB, and compared the resulting orbital evolution with the RKF integrations. We use the same evolutionary track as in Sec. 3.2. The bottom panel of Fig. 5 shows results for a set of simulations developed for a Jupiter-mass planet with different initial separations between 2.3 au and 3.1 au. It is clear that both kinds of integrations almost perfectly match. The eccentricity of these Jupiter-mass planets was initially set to be 0.1 in order to also test the changes in this orbital parameter. The top panel of Fig. 5 also shows a nearly perfect match in the evolution of the eccentricities.

REFERENCES

- Antoniadou, K. I., & Veras, D. 2019, *A&A*, 629, A126, doi: [10.1051/0004-6361/201935996](https://doi.org/10.1051/0004-6361/201935996)
- Barber, S. D., Patterson, A. J., Kilic, M., et al. 2012, *ApJ*, 760, 26, doi: [10.1088/0004-637X/760/1/26](https://doi.org/10.1088/0004-637X/760/1/26)

- Barstow, M. A., Barstow, J. K., Casewell, S. L., Holberg, J. B., & Hubeny, I. 2014, *MNRAS*, 440, 1607, doi: [10.1093/mnras/stu216](https://doi.org/10.1093/mnras/stu216)
- Beauge, C., & Ferraz-Mello, S. 1993, *Icarus*, 103, 301, doi: [10.1006/icar.1993.1072](https://doi.org/10.1006/icar.1993.1072)
- Beaugé, C., Michtchenko, T. A., & Ferraz-Mello, S. 2006, *MNRAS*, 365, 1160, doi: [10.1111/j.1365-2966.2005.09779.x](https://doi.org/10.1111/j.1365-2966.2005.09779.x)
- Chambers, J. E. 1999, *MNRAS*, 304, 793, doi: [10.1046/j.1365-8711.1999.02379.x](https://doi.org/10.1046/j.1365-8711.1999.02379.x)
- Fabrycky, D. C., Ford, E. B., Steffen, J. H., et al. 2012, *ApJ*, 750, 114, doi: [10.1088/0004-637X/750/2/114](https://doi.org/10.1088/0004-637X/750/2/114)
- Folonier, H. A., Roig, F., & Beaugé, C. 2014, *Celestial Mechanics and Dynamical Astronomy*, 119, 1, doi: [10.1007/s10569-014-9542-y](https://doi.org/10.1007/s10569-014-9542-y)
- Frewen, S. F. N., & Hansen, B. M. S. 2014, *MNRAS*, 439, 2442, doi: [10.1093/mnras/stu097](https://doi.org/10.1093/mnras/stu097)
- Gänsicke, B. T., Schreiber, M. R., Toloza, O., et al. 2019, *Nature*, 576, 61, doi: [10.1038/s41586-019-1789-8](https://doi.org/10.1038/s41586-019-1789-8)
- Gänsicke, B. T., Aungwerojwit, A., Marsh, T. R., et al. 2016, *ApJL*, 818, L7, doi: [10.3847/2041-8205/818/1/L7](https://doi.org/10.3847/2041-8205/818/1/L7)
- Gillon, M., Triaud, A. H. M. J., Demory, B.-O., et al. 2017, *Nature*, 542, 456, doi: [10.1038/nature21360](https://doi.org/10.1038/nature21360)
- Giuppone, C. A., Morais, M. H. M., & Correia, A. C. M. 2013, *MNRAS*, 436, 3547, doi: [10.1093/mnras/stt1831](https://doi.org/10.1093/mnras/stt1831)
- Gladman, B. 1993, *Icarus*, 106, 247, doi: [10.1006/icar.1993.1169](https://doi.org/10.1006/icar.1993.1169)
- Hurley, J. R., Pols, O. R., & Tout, C. A. 2000, *MNRAS*, 315, 543, doi: [10.1046/j.1365-8711.2000.03426.x](https://doi.org/10.1046/j.1365-8711.2000.03426.x)
- Jones, M. I., Jenkins, J. S., Brahm, R., et al. 2016, *A&A*, 590, A38, doi: [10.1051/0004-6361/201628067](https://doi.org/10.1051/0004-6361/201628067)
- Jura, M. 2003, *ApJL*, 584, L91, doi: [10.1086/374036](https://doi.org/10.1086/374036)
- Koester, D., Gänsicke, B. T., & Farihi, J. 2014, *A&A*, 566, A34, doi: [10.1051/0004-6361/201423691](https://doi.org/10.1051/0004-6361/201423691)
- Malamud, U., & Perets, H. B. 2020, *MNRAS*, 492, 5561, doi: [10.1093/mnras/staa142](https://doi.org/10.1093/mnras/staa142)
- Manser, C. J., Gänsicke, B. T., Gentile Fusillo, N. P., et al. 2020, *MNRAS*, 493, 2127, doi: [10.1093/mnras/staa359](https://doi.org/10.1093/mnras/staa359)
- Manser, C. J., Gänsicke, B. T., Eggl, S., et al. 2019, *Science*, 364, 66, doi: [10.1126/science.aat5330](https://doi.org/10.1126/science.aat5330)
- Mordasini, C. 2018, *Planetary Population Synthesis*, 143, doi: [10.1007/978-3-319-55333-7_143](https://doi.org/10.1007/978-3-319-55333-7_143)
- Mustill, A. J., & Villaver, E. 2012, *ApJ*, 761, 121, doi: [10.1088/0004-637X/761/2/121](https://doi.org/10.1088/0004-637X/761/2/121)
- Nordhaus, J., & Spiegel, D. S. 2013, *MNRAS*, 432, 500, doi: [10.1093/mnras/stt569](https://doi.org/10.1093/mnras/stt569)
- Pfytter, S., Alibert, Y., Benz, W., & Swoboda, D. 2015, *A&A*, 579, A37, doi: [10.1051/0004-6361/201424295](https://doi.org/10.1051/0004-6361/201424295)
- Ramos, X. S., Correa-Otto, J. A., & Beaugé, C. 2015, *Celestial Mechanics and Dynamical Astronomy*, 123, 453, doi: [10.1007/s10569-015-9646-z](https://doi.org/10.1007/s10569-015-9646-z)
- Rao, S., Meynet, G., Eggenberger, P., et al. 2018, *A&A*, 618, A18, doi: [10.1051/0004-6361/201833107](https://doi.org/10.1051/0004-6361/201833107)
- Rasio, F. A., Tout, C. A., Lubow, S. H., & Livio, M. 1996, *ApJ*, 470, 1187, doi: [10.1086/177941](https://doi.org/10.1086/177941)
- Reimers, D. 1975, *Memoires of the Societe Royale des Sciences de Liege*, 8, 369
- Ronco, M. P., & de Elía, G. C. 2018, *MNRAS*, 479, 5362, doi: [10.1093/mnras/sty1773](https://doi.org/10.1093/mnras/sty1773)
- Ronco, M. P., Guilera, O. M., & de Elía, G. C. 2017, *MNRAS*, 471, 2753, doi: [10.1093/mnras/stx1746](https://doi.org/10.1093/mnras/stx1746)
- Schneider, J., Dedieu, C., Le Sidaner, P., Savalle, R., & Zolotukhin, I. 2011, *A&A*, 532, A79, doi: [10.1051/0004-6361/201116713](https://doi.org/10.1051/0004-6361/201116713)
- Schreiber, M. R., Gänsicke, B. T., Toloza, O., Hernandez, M.-S., & Lagos, F. 2019, *ApJL*, 887, L4, doi: [10.3847/2041-8213/ab42e2](https://doi.org/10.3847/2041-8213/ab42e2)
- Shallue, C. J., & Vanderburg, A. 2018, *AJ*, 155, 94, doi: [10.3847/1538-3881/aa9e09](https://doi.org/10.3847/1538-3881/aa9e09)
- Smallwood, J. L., Martin, R. G., Livio, M., & Lubow, S. H. 2018, *MNRAS*, 480, 57, doi: [10.1093/mnras/sty1819](https://doi.org/10.1093/mnras/sty1819)
- Suzuki, D., Bennett, D. P., Sumi, T., et al. 2016, *ApJ*, 833, 145, doi: [10.3847/1538-4357/833/2/145](https://doi.org/10.3847/1538-4357/833/2/145)
- Trifonov, T., Reffert, S., Tan, X., Lee, M. H., & Quirrenbach, A. 2014, *A&A*, 568, A64, doi: [10.1051/0004-6361/201322885](https://doi.org/10.1051/0004-6361/201322885)
- Vanderburg, A., Johnson, J. A., Rappaport, S., et al. 2015, *Nature*, 526, 546, doi: [10.1038/nature15527](https://doi.org/10.1038/nature15527)
- Veras, D. 2016, *Royal Society Open Science*, 3, 150571, doi: [10.1098/rsos.150571](https://doi.org/10.1098/rsos.150571)
- Veras, D., Eggl, S., & Gänsicke, B. T. 2015, *MNRAS*, 451, 2814, doi: [10.1093/mnras/stv1047](https://doi.org/10.1093/mnras/stv1047)
- Veras, D., & Fuller, J. 2020, *MNRAS*, 492, 6059, doi: [10.1093/mnras/staa309](https://doi.org/10.1093/mnras/staa309)
- Veras, D., & Gänsicke, B. T. 2015, *MNRAS*, 447, 1049, doi: [10.1093/mnras/stu2475](https://doi.org/10.1093/mnras/stu2475)
- Veras, D., Leinhardt, Z. M., Bonsor, A., & Gänsicke, B. T. 2014, *MNRAS*, 445, 2244, doi: [10.1093/mnras/stu1871](https://doi.org/10.1093/mnras/stu1871)
- Veras, D., Mustill, A. J., Bonsor, A., & Wyatt, M. C. 2013, *MNRAS*, 431, 1686, doi: [10.1093/mnras/stt289](https://doi.org/10.1093/mnras/stt289)
- Villaver, E., & Livio, M. 2009, *ApJL*, 705, L81, doi: [10.1088/0004-637X/705/1/L81](https://doi.org/10.1088/0004-637X/705/1/L81)
- Villaver, E., Livio, M., Mustill, A. J., & Siess, L. 2014, *ApJ*, 794, 3, doi: [10.1088/0004-637X/794/1/3](https://doi.org/10.1088/0004-637X/794/1/3)
- Voyatzis, G., Hadjidemetriou, J. D., Veras, D., & Varvoglis, H. 2013, *MNRAS*, 430, 3383, doi: [10.1093/mnras/stt137](https://doi.org/10.1093/mnras/stt137)
- Zahn, J. P. 1977, *A&A*, 500, 121

Zhu, W., Petrovich, C., Wu, Y., Dong, S., & Xie, J. 2018,
ApJ, 860, 101, doi: [10.3847/1538-4357/aac6d5](https://doi.org/10.3847/1538-4357/aac6d5)

Zink, J. K., Christiansen, J. L., & Hansen, B. M. S. 2019,
MNRAS, 483, 4479, doi: [10.1093/mnras/sty3463](https://doi.org/10.1093/mnras/sty3463)